ELSEVIER

Advances in Water Resources 24 (2001) 1103–1118

Advances in Water Resources

www.elsevier.com/locate/advwatres

Relative importance of local and regional controls on coupled water, carbon, and energy fluxes

John D. Albertson [a,*], Gabriel G. Katul [b], Patricia Wiberg [a]

[a] *Department of Environmental Sciences, University of Virginia, Charlottesville, VA 22903, USA*
[b] *Nicholas School of the Environment, Duke University, USA*

Received 19 July 2000; received in revised form 13 February 2001; accepted 14 March 2001

Abstract

This paper reports the first effort to include carbon, water, and heat exchange in a Large Eddy Simulation (LES) model for 3D canopy flows with dynamic response of leaf temperature and stomatal aperture. The LES model simulates eddy motion from 3D, transient integration of a filtered form of the Navier–Stokes equations. Carbon exchange between the vegetation and air is predicted in space and time following biophysical considerations, which act to maximize carbon assimilation while minimizing water loss. The vegetation's stomatal conductance is inferred from these same considerations and used to regulate both transpiration and carbon assimilation rates. Variations in transpiration and radiation distribution propagate to foliage temperature and ultimately heat exchange through a local, transient vegetation energy balance. The wind field is affected by the foliage patterns and by the temperature profile's control on vertical mixing. These temperature and mixing patterns control the concentration profiles that, in turn, affect water and CO_2 exchange processes. By comparing a simulation of horizontally heterogeneous canopy behavior to simulations of several homogeneous canopies with different leaf area index (LAI) values we evaluate the relative importance of local and regional LAI values on the local microenvironment variables and fluxes from the forest canopy. We focus on a pine forest with ample soil moisture as a case study. We demonstrate from these simulations that primitive state variables (e.g. concentrations and velocity) exhibit noticeable non-local controls. However, these features are offset in their effects on land surface fluxes, such that the local fluxes scale well with local LAI values. Furthermore, the resulting relationships between LAI and fluxes are quasi-linear (for the forest morphology studied here) allowing for robust relationships between forest averaged LAI and forest averaged fluxes. The offsetting nature of the non-local effects is described in the context of the dual regulation of stomatal conductance by the rates of carbon assimilation and water loss as opposed to independent regulating effects of the various state variables. Hence, non-local variations in state variables naturally induce offsetting variations in stomatal conductance thereby buffering the water use efficiency of the plant from environmental excursions associated with the turbulent microclimate.

1. Introduction

The exchange of energy, water, and CO_2 between vegetated land surfaces and the atmosphere plays a central role in the dynamics of weather, climate, surface hydrology, and terrestrial ecology. The exchange rates are regulated and affected by an intertwined collection of physical, biological, and chemical processes. These processes possess varying degrees of non-linearity and scale dependencies with respect to forcing variables. We focus here on elucidating some of these issues for mass and energy exchanges within and over forest canopies.

It has long been recognized that the addition of an energy balance to the water balance constrains estimation of evaporative fluxes. However, the dependence of transpiration on stomatal aperture frustrates closure of the equations. A common modeling approach in hydrology has been to adopt a maximum stomatal conductance for a given vegetation type and then reduce this amount through independent empirical reduction functions that vary with an array of environmental factors, such as temperature and vapor pressure deficit (VPD) [26]. More recent advances in the ecophysiology community suggest that stomatal conductance responds directly to the rate of carbon assimilation inside the leaf [9,13,22,50–52], with a general optimization strategy that seeks to maximize carbon gain while minimizing water loss [14]. Since the carbon assimilation rate involves temperature dependent biochemical reactions

* Corresponding author. Tel.: +1-804-924-7241; fax: +1-804-982-2137.
E-mail address: albertson@virginia.edu (J.D. Albertson).

0309-1708/01/$ - see front matter
PII: S0309-1708(01)00042-2

and is driven by solar energy and since the water loss is driven by vapor pressure gradients across the leave surface, the stomatal aperture is defined by the concerted influences of water, carbon, and energy states. Hence, the addition of carbon balance considerations to the water and energy balances provides an added equation to match the number of unknowns, and hence close the system of equations in a way that resolves the intertwined dynamics of the water, carbon, and energy cycles in the above ground portion of terrestrial systems.

Incident solar radiation excites the exchange processes at the leaf-level and turbulent transport re-distributes the mass and energy throughout the atmospheric boundary layer (ABL), thus influencing concentration gradients between the foliage and the air. The "coarse scale" geometry of the plant canopy not only defines the distribution of the leaf area, but it also affects the distribution of solar radiation and turbulent mixing throughout the canopy. In a local sense (i.e. considering only collocated variables) the concentration of leaf surface area provides a potential source or sink of mass, momentum, and energy for the atmosphere; and, in a non-local sense (i.e. depending on remote or regional variables), the regionally aggregated canopy properties contribute to the regional air properties and wind field. The combined action of these local and non-local controls defines the exchange rates, which then interact with the turbulent mixing to alter the microclimate and potentially feedback on the biophysical processes within the individual leaves.

Conceptually, we can consider separately the effects of the vertical and horizontal distribution of canopy density. Problems related to horizontal variability range from small-scale issues such as shading of adjacent trees under low sun angles to well-known issues of advection under spatial variability of land surface properties (e.g. [2,3,7,8,25]). Vertical canopy structure exerts the omnipresent control on radiation penetration and mixing between concentrations of carbon, water vapor, and heat within and above the canopy (e.g. [12,30,43,53]). What remains illusive is a robust and parsimonious means to represent the net impact of these processes at the larger scale. Motivation to seek simplifying rules for the estimation of landscape scale fluxes is provided by theoretical studies that have focused on a limited number of variables. For example, McNaughton and Jarvis [36] found that conditions of reduced atmospheric mixing in the canopy (low laminar boundary layer conductances) can lead to a reduced sensitivity of canopy scale transpiration to stomatal conductance. If the relative influences of meteorological forcing and vegetation structure on coupled exchange phenomena are defined at the landscape scale, then the potential exists to combine remotely observed vegetation density data and meteorological factors to estimate real-time and future fluxes of water, heat, and carbon over realistic land surfaces.

Our objective is to investigate how variability in foliage distribution interacts with turbulent mixing, radiative exchange, and leaf physiology to induce variability in land surface fluxes. Towards this end we consider both horizontal and vertical variation in foliage in the presence of shear and buoyancy driven turbulent flow. We approach the problem with the state of the art in numerical simulation of canopy turbulence, using the Large Eddy Simulation (LES) technique. With the LES technique, resolved eddies are "simulated" in three spatial dimensions through time by direct integration of the Navier–Stokes equations filtered to the scale of the numerical mesh. The effect of the small-scale field (subgrid) on the resolved (flux carrying) eddies is "modeled" through a subgrid eddy viscosity. Hence, the important dynamics of the air and the resulting transport follow from the Navier–Stokes equations. Although LES has been successfully applied to simulate canopy flows [19,45,47,48], this is the first investigation to include water vapor, carbon, and heat exchanges that are based on a dynamical coupling of leaf and air properties. The simulations use a canopy-affected radiation distribution and a dynamic vegetation energy balance, which considers changes in leaf heat storage due to imbalances between net radiation and the fluxes of sensible and latent heat from the canopy to the surrounding air. This case study focuses on pine as the vegetation type, adopting appropriate biophysical parameters, and we explore horizontally heterogeneous and homogeneous leaf area index (LAI) cases. Our analysis is limited to this pine monoculture with ample soil moisture and its simulated response over a single mid-day period.

In addition to these spatial scale interactions there are important temporal scaling issues to be dealt with. In a separate paper in this issue [31] we explore key features of the relationships between the meteorological forcing and land surface fluxes in the time domain over time scales ranging from seconds to years.

2. Theory

In this section we summarize the mathematical basis of the turbulence simulation, the radiation distribution, the leaf-level biophysics and the integration of these coupled processes to the landscape scale.

2.1. Large Eddy Simulation

The LES technique was pioneered by Deardorff [15,16] and applied successfully to simulate the convective boundary layer. The approach has recently been shown to capably simulate the neutrally stratified ABL as well [5]. These codes have also shown how heterogeneous properties of a planar surface affect boundary

layer flows [2,3,24,46] and how wavy terrain induces effects on the turbulent fluxes [33]. But, perhaps most promising for the present objectives, the pioneering study of Shaw and Schumann [45] proved that the LES technique is useful for exploring turbulent flow over and through a forest canopy. The important flow and transport features were reproduced well by their simulations.

With the LES technique the resolved eddies are simulated by a space-time integration of the Navier–Stokes equations filtered to the scale of the numerical mesh. The fluxes between the vegetation and the air are distributed in space and time as instantaneous functions of the local canopy state, the state of the air in contact with the vegetation, and available energy (physiological processes are described below). The transient velocity field interacts with transient scalar fields to affect scalar flux fields throughout the canopy space and above.

The LES technique is a major departure from conceptual models of turbulent transport, such as the Reynolds-averaged models (e.g. [29]) used in many 1D multi-level canopy models (e.g. [34]), where all the turbulence is averaged out and represented in total by a closure model. The Reynolds averaged approaches are especially problematic when applied to plant canopies because of their difficulty in dealing with fluxes that are not proportional to local gradients (e.g. see [17,44]). These effects of the eddy dynamics in the canopy are simulated naturally (implicitly) with the LES approach.

The LES code used here was originally developed for ABL simulations under neutral conditions [1,2], extended to handle ABL simulations under convective conditions [3], adapted to handle remotely sensed land surface conditions [4], and recently adapted to handle embedded plant canopies with radiation, dynamic foliage energy balances, and carbon exchange and transport as described here.

The canopy LES code integrates filtered equations, based on conservation of momentum and mass for a turbulent fluid with embedded vegetation:

$$\partial_i u_i = 0, \tag{1}$$

$$\partial_0 u_i + u_j\left(\partial_j u_i - \partial_i u_j\right) = -\partial_i p - \partial_j \tau_{ij} + \beta\delta_{i3} - f_i, \tag{2}$$

$$\partial_0 \theta + u_j \partial_j \theta = -\partial_j \pi_j^{\theta} + h, \tag{3}$$

$$\partial_0 q + u_j \partial_j q = -\partial_j \pi_j^{q} + e, \tag{4}$$

$$\partial_0 c + u_j \partial_j c = -\partial_j \pi_j^{c} + \eta, \tag{5}$$

where u_i is the filtered (or resolved) velocity component in the x_i direction ($x_1 = x, x_2 = y,\ x_3 = z$), p is the pressure (which includes the trace of the turbulent kinetic energy and the trace of the subgrid stress tensor, and is normalized by the density), τ_{ij} is the subgrid stress tensor (arising from the filtering of the equations to the mesh), f_i is a local drag term arising from the vegetation inside the grid cell, $\beta(=(\theta - \langle\theta\rangle)/\theta)$ is the buoyancy term that connects the temperature equation to the vertical momentum equation and accounts for the dynamic effects of the density stratification, $\langle\cdot\rangle$ is a horizontal averaging operator, δ_{ij} is the Kronecker delta, θ is the potential air temperature, q is the specific humidity, c is the concentration of CO_2, π_j^{θ} is the subgrid flux of temperature in the j direction, h is a local source term for heat exchanged with the vegetation, π_j^{q} is the subgrid flux of humidity in the j direction, e is a local source term for water vapor exchanged with the vegetation, π_j^{c} is the subgrid flux of CO_2 in the j direction, and η is a local source term for CO_2 exchanged with the canopy ($\eta < 0$ for canopy uptake). All the equations are made dimensionless by appropriate large-scale variables and Einstein's summation is implied by repeated subscripts. The source/sink terms (f_i, h, e, η) are described in Section 2.3.

This is the first published LES study to include CO_2 exchange with vegetation induced by a coupling of radiation and photosynthesis in thermodynamically active vegetation. This is a departure from the previous approaches using LES for canopy (e.g. [45]), where a prescribed homogeneous scalar source strength was employed.

The equations are integrated in space and time using a mixed pseudospectral numerical technique [2], thus generating a coarse-grained view of the interaction of the atmosphere and the canopy, the dynamics of flow inside the canopy, and the connection between this portion of the flow with the free air above. The mixed pseudospectral approach for the numerical solution employed in our code was first used for turbulent channel flow by Moin et al. [39], and then later for the ABL by Moeng [38]. Our version builds on the work of Moin et al., with several advances to handle canopy sublayer flows.

2.2. Radiation

The leaf energy balance interacts directly with the net radiation (R_n), including both long (terrestrial and atmospheric) and short (solar) wave fluxes. However, the carbon assimilation rates are constrained by the available photosynthetically active radiation (PAR), which consists of a fraction of the short wave flux (between 400 and 700 nm). We distribute both R_n and PAR vertically through the canopy with a 1D radiative transmission algorithm [11, p. 255] that approximates the (high order) binomial probability of radiation interception by the Poisson distribution, which results in a simple exponential function of leaf density at each x–y position. As we simulate a pine canopy we use a leaf clumping factor of 0.8 and an absorbtivity for the R_n of 0.5 [11]. This distributed 1D approach is acceptable since our simulations consider cases with high sun angles and where the length scale of horizontal variability is greater than the depth of the canopy. Hence, the local leaf area density profile shape dictates the vertical distribution of

PAR and R_n. This approach is a first-order simplification that cannot capture different photosynthetic responses to direct and diffuse radiation. However, our intent here is to resolve dominant effects of solar radiation with reasonable dependence on canopy geometry.

2.3. Leaf-level fluxes

The velocity field is subject to a local momentum sink (f_i) that depends on the vegetation density and the wind speed and direction according to

$$f_i = C_d a V u_i, \tag{6}$$

where a [m_l^2 m^{-3}] is the local vegetation density (varies in x,y,z), V is the scalar wind speed (i.e. $(u_1^2 + u_2^2 + u_3^2)^{1/2}$), and C_d ($=0.15$) is an empirical drag coefficient [45].

The sensible heat exchange between the vegetation and air is estimated by

$$h = a g_b(\theta_l - \theta), \tag{7}$$

where g_b is a conductance to heat transfer across the laminar boundary layer on a leaf that is $\propto \sqrt{V/l}$, where l is a characteristic leaf length [11, p. 101], and θ_l and θ are the leaf surface and local air temperatures, respectively. All variables in (7) are functions of (x,y,z,t), with the leaf temperature evolving according to a foliage energy balance (discussed below) and the air temperature described by (3).

Within canopy water vapor exchange is dependent on the stomatal conductance, which we derive from considerations of the carbon assimilation processes [14,22]. The local net rate of carbon uptake (η) is determined by biochemical reactions and by diffusion from the ambient air to the chloroplast, where the biochemical reactions are either limited by the amount of absorbed PAR (i.e. electron transport dependence on photon flux) or by the enzyme kinetics of the ribulose biphosphate carboxylase–oxygenase (Rubisco), as described by Farquhar et al. [22], hence

$$\eta = \min\left(A_{par}, A_{ru}\right) a. \tag{8}$$

The PAR limited rate is estimated as

$$A_{par} = \frac{\alpha_{par}\varepsilon_{max} Q_{par}(C_i - \Gamma)}{C_i + 2\Gamma} - R_d, \tag{9}$$

where A_{par} has units of μmol m_l^{-2} s^{-1}, with m_l^{-2} implying per square meter of leaf area, α_{par} ($=0.9$) is the absorbtivity of the leaf with respect to PAR, ε_{max} ($=0.08$) is the maximum ratio of molecules of CO_2 fixed per quantum of PAR absorbed, Q_{par} is the PAR photon flux density [μmol m_l^{-2} s^{-1}], C_i is the CO_2 concentration inside the leaf [μmol mol^{-1} or parts per million), Γ is the CO_2 compensation point, which is the minimum C_i for which there is finite assimilation, and R_d (μmol m_l^{-2} s^{-1}) is the dark respiration rate. The Rubisco limited rate is estimated (after [22]) as

$$A_{ru} = V_{c\max}\left(\frac{C_i - \Gamma}{C_i + k_c\left(1 + \frac{O_i}{k_o}\right)}\right) - R_d, \tag{10}$$

where $V_{c\max}$ (μmol m_l^{-2} s^{-1}) is the maximum catalytic activity of Rubisco with saturating RuBP, O_i (ppm) is the intercellular O_2 concentrations, and k_c and k_o are the Michaelis coefficients (ppm) of Rubisco for CO_2 and O_2, respectively. The temperature dependencies of the kinetic parameters k_c, k_o, and R_d are calculated as described in De Pury and Farquhar [18] and Medlyn et al. [37] and repeated below. See Table 1 for further detail.

$$\begin{aligned}
V_{c\max}(\theta_l) &= V_{c\,max}^{ref} \exp\left(\frac{E_{v\max}(\theta_l - 25)}{298R(\theta_l + 273)}\right),\\
\Gamma &= 36.9 + 1.88(\theta_l - 25) + 0.036(\theta_l - 25)^2,\\
k_c &= k_c^{ref} \exp\left(\frac{E_{ac}(\theta_l - 25)}{298R(\theta_l + 273)}\right),\\
k_o &= k_o^{ref} \exp\left(\frac{E_{ao}(\theta_l - 25)}{298R(\theta_l + 273)}\right).
\end{aligned} \tag{11}$$

Table 1
Eco-physiological variables for estimating g_c for pine [31]

Variable	Value	Note
D_o	296.7 (ppm)	Estimated from porometry measurements [31]
m_L	3.54 (dimensionless)	Estimated from porometery measurements as in Katul et al. [31]
Γ	80 ppm	Estimated from measured Light-Response curves [21]
$V_{c\max}^{ref}$	98.9 (μmol m^{-2} s^{-1})	Estimated from measured Light-Response curves
O_i	210,000 ppm	From [18,37]
R_d	0.015 $V_{c\max}$ (T)	From [22,23]
$E_{v\max}$	68,000 $°C^{-1}$	
R	8.314	
E_{ac}	59,400 $°C^{-1}$	
E_{ao}	36,000 $°C^{-1}$	
k_c^{ref}	404 ppm	
k_o^{ref}	248,000 ppm	

Note: The polynomial for Γ (in ppm) is from [28].

Hence, the assimilation rate A depends on the vegetation temperature and C_i. From the diffusion of CO_2 through the stomatal pores there is an implicit relationship between η and C_i

$$\eta = -g_c(C_i - C_s)a, \tag{12}$$

where g_c [mol m_l^{-2} s^{-2}] is the stomatal conductance with respect to CO_2 diffusion and C_s is the concentration of CO_2 at the outer leaf surface, which is related to the concentration in the free air by the leaf boundary layer conductance. Since we have one more unknown than equations, we turn to an expression describing controls of g_c.

Wong et al. [50–52] demonstrated the strong relationship between g_c and the carbon assimilation rate. In consideration of this, Ball et al. [9] proposed a relationship for g_c that accounted for the influences of carbon assimilation rate, C_s, and relative humidity. However, subsequent experiments [40] revealed that stomata respond to intercellular CO_2 concentration and not to leaf surface concentrations or ambient concentrations. There has also been debate about the functional controls of aridity on stomatal aperture, with Ball et al. [9] suggesting dependence on relative humidity of the air, Aphalo and Jarvis [6] concluding from experiments that VPD is more appropriate than relative humidity and, finally, Mott and Parkhurst [41] demonstrating from the results of a novel experiment that it is actually the *rate of water loss* through the stomatal pores that governs the response. However, given its strong relationship to transpiration, the VPD persists as the dominant choice of variables to serve as a proxy for rate of water loss in the mathematical description of conductance. The influence of soil moisture on stomatal conductance is often neglected in ecological applications (e.g. [13]); however, it can become important under drought conditions [42] because it induces hydraulic failure by cavitation in the root-xylem pathway. In this first study, we focus on non-water-limiting conditions and therefore omit soil moisture status from the functional description of g_c. With this in mind, we adopt the approach of Leuning [35] for describing the controls on stomatal conductance

$$g_c = m_L\left(\frac{Af_L(D)}{(C_s - \Gamma)}\right) + g_o, \quad f_L(D) = \frac{1}{1 - \frac{D}{D_o}}, \tag{13}$$

where m_L is an empirically derived species-specific constant, $A = \min(A_{ru}, A_{par})$, C_s is used as a proxy for C_i since it is the more readily measured field quantity via porometry (and is related to C_i via g_c), D is the vapor pressure deficit (or VPD), D_o is an empirical constant describing the species sensitivity to VPD, and g_o is the residual conductance at $A = 0$. Leuning [35] and later Katul et al. [31] demonstrated that the formulation in (13) better reproduces A measured by porometry when contrasted with the Ball–Berry type formulation.

The equations in this section may be solved iteratively or closed with a minor approximation. The iterative approach would be to estimate C_i (typically it is found to be proportional to C_s or C_a, [20], calculate A from (9)–(11), compute g_c from (13), revise the estimate of C_i from (12) and continue iteration until convergence. A reasonable closure approximation (which was used in this study) is to ignore g_o, thus allowing direct calculation of C_i from the combination of (13) and (12) as

$$C_i = C_s - \left(\frac{C_s - \Gamma}{m_L f_L(D)}\right) \tag{14}$$

and then proceeding with the direct calculation of A and g_c. Note that $D(x, y, z, t)$ is available from (3) and (4).

The stomatal conductance for water vapor (transpiration) is approximately 1.56 times greater than that for CO_2, due to the different molecular diffusivities of the two gases in air [11]. Hence, we estimate the water vapor source terms as

$$e = \left(1.56 g_c m_a \rho_a^{-1}\right)(q^*(\theta_l) - q_s)a, \tag{15}$$

where m_a is the molecular weight of air, ρ_a is the density of air, $q^*(\theta_l)$ is the saturated specific humidity (g kg^{-1}) at the leaf temperature and q_s is the specific humidity of the air at the surface of the leaf, which is related to q via a laminar leaf boundary layer conductance analogous to the treatment of sensible heat exchange.

The temperature of the foliage at each computational node evolves in response to a local vegetation energy balance

$$\frac{\partial \theta_l}{\partial t} = \frac{1}{\rho_l c_p (adz)}[R_n - h - L_v e], \tag{16}$$

where ρ_l (= 2.4 kg ml^{-2}) is the mass of foliage per unit leaf area, c_p (= 4190 J kg^{-1} K^{-1}) is the specific heat capacity of the foliage, L_v (= 2450 J g^{-1}) is the latent heat of vaporization, and dz is the vertical node spacing, such that adz has units of [m_l^2 m^{-2}].

2.4. Integration

With this representation of canopy fluxes, the spatial variability in canopy structure ($a(x, y, z)$ [m_l^2 m^{-3}]) gives rise to variable net radiation penetration within the canopy space (and corresponding density stratification), variable water vapor, heat, CO_2, and momentum exchange with the turbulent air flow (6)–(16). The variable fluxes, consequently, inject variability into the velocity, temperature, humidity, and CO_2 fields flowing through the canopy (2)–(5). The simulations are 3D, with 32 nodes in the X direction (streamwise), 32 nodes in the Y direction (spanwise) and 100 nodes in the vertical direction, for a total of 102,400 computational nodes. The simulation domain covers 100 m in the vertical direction and 200 m in each the x and y directions. The numerical solutions march forward on a time step of less than 1 s. Fields of primitive variables (e.g. $u_i, C, q \ldots$), fluxes (e.g. $u_3 q, u_3 C, \ldots$), and variances are time averaged for anal-

ysis of relationships between spatial distribution of vegetation density and spatial distribution of mass and energy fluxes.

3. Simulations

The 3D geometry of the canopy is expressed in terms of horizontal LAI maps and a vertical shape function, such that

$$a(x,y,z) = \mathrm{LAI}(x,y) * \lambda(z), \tag{17}$$

where λ serves to distribute the leaf area in the vertical for any position in the x-y plane. We use the measured vertical shape of the Duke Forest [20]. The vertical shape used in all cases and the horizontal distribution of LAI used in the horizontally heterogeneous case are shown in Fig. 1. Note the secondary peak in the vertical shape, where the foliage density is approximately one-half that of the primary peak. We refer back to this when examining the relationships between the canopy shape and the shapes of the source/sink profiles in the results. Note also that the canopy is embedded in the bottom 1/6th of the flow simulation domain (100 m). The horizontally heterogeneous case has LAI ranging from 3.7 to 7.6 $m_l^2\ m^{-2}$ (consistent with the measured spatial variation in LAI reported in [32]) and was generated as a random field from an exponential correlation model with a prescribed spatial correlation length of about two times the canopy height (see Fig. 1(b)). For each case the canopy density geometry was generated and embedded in the LES. Table 2 summarizes the canopy geometry of the four cases. The contrast between Cases 1 and 3 reflects heterogeneous versus homogeneous horizontal canopy structure. Cases 2 and 4 allow an examination of the relative contribution of local and non-local effects in the LAI versus flux distributions derived in Case 1. For example, we can compare fluxes from local regions of $\mathrm{LAI} = 4$ (or $\mathrm{LAI} = 7$) in a global field that has a mean canopy LAI of 5.5 (in Case 1) with results from Case 2 (or Case 4)

Table 2
Characterization of foliage structure for the simulation cases

	Horizontal structure[a], α	Vertical shape[b], λ
Case 1	Variable, $\langle \mathrm{LAI} \rangle = 5.5, L_a = 30$ m	Pine forest
Case 2	Homogeneous, LAI = 4	Pine forest
Case 3	Homogeneous, LAI = 5.5	Pine forest
Case 4	Homogeneous, LAI = 7	Pine forest

[a] Simulated forest size is 200 m × 200 m (see Fig. 1).
[b] Canopy height = 14 m, all cases (see Fig. 1).

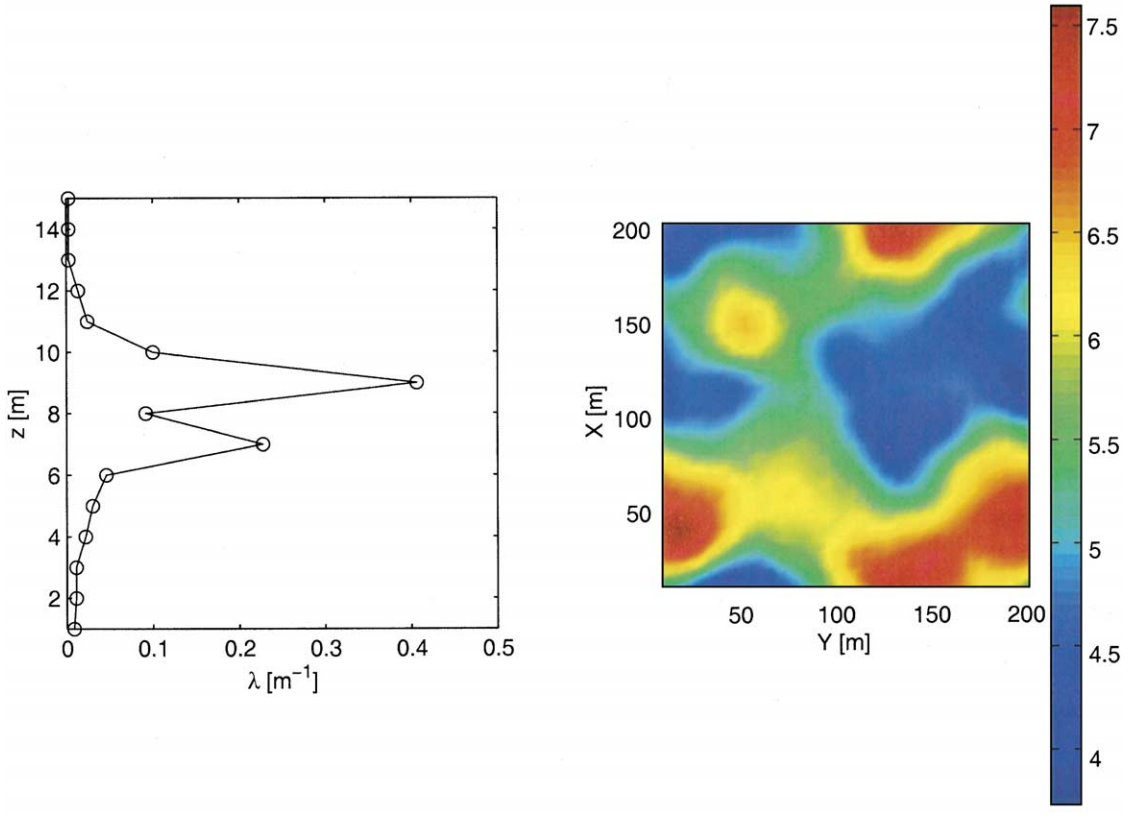

Fig. 1. The left panel shows the normalized vertical shape function of the pine canopy (shape function). The right panel depicts the horizontal distribution of leaf area density used in the heterogeneous canopy simulation.

Table 3
Boundary conditions and forcing of the simulation

Boundary or forcing	Treatment
Horizontal (flow BC)	Periodic
Upper (flow BC)	Stress-free and zero-flux. At 100 m[a]
Net radiation[b]	500 W m_g^{-2}, horizontally uniform
Photosynthetically active radiation[b]	1200 μmol m_g^{-2} s^{-1}
Mean kinematic pressure forcing[c]	9E − 4 m s^{-2}
Upper ABL CO_2 concentration	360 μmol mol^{-1}

[a] Partial simulation of ABL depth, thus omitting boundary layer scales eddies.
[b] Total to distribute between canopy and soil at each x, y location.
[c] General longitudinal flow forcing.

where the entire global field is LAI = 4 (or LAI = 7). Table 3 summarizes the boundary conditions for the flow simulation and the regional forcing characteristics with respect to pressure gradient and radiation.

4. Results and discussion

In this section we present the simulation results of the cases in Table 2 and discuss the effects of foliage distribution on the variability in land–atmosphere fluxes. Given that the scalar sources and sinks are dependent on the flow statistics, we first address the impact of foliage distribution on the mean flow field. The effects of leaf area density distribution on scalar sources and fluxes within the canopy are considered next. Finally, we progress to derive functional relationships between vegetation density (LAI) and exchange rates of water, heat, and carbon. These relationships permit us to assess the combination of local and global scaling measures that are needed to describe variability in canopy fluxes.

4.1. Velocity field

In Fig. 2 we present the mean wind speed for each of the four cases plotted versus height in the lower 30 m (i.e. $2h$, where h is canopy height) of the flow domain. The concept of a zero-plane displacement (e.g. [10, p. 116]) is evident in the figure, with weak mean winds in the region below the peak foliage density. In these profiles and the profile figures to follow, the LES flow variables (which vary over x, y, z, t) have been time averaged over 30-min and horizontally averaged (over the full x, y domain), such that the resulting means are only functions of z. When subjected to the same mean pressure gradient, the heterogeneous and homogeneous cases with $\langle \mathrm{LAI} \rangle = 5.5$ have similar wind speeds inside the canopy, however above the canopy the heterogeneous case has a lower $\langle U \rangle$. This is expected because the presence of a heterogeneous surface roughness is known to result in greater regional shear stress due to asymmetrical response of the wind field to rough-to-smooth and smooth-to-rough transitions [3]. For the homogeneous cases, an increase in LAI results in a decrease in wind speed in the lower canopy (understory) and an increase in wind speed above the canopy. This is due to a 'skimming effect' of the wind over a dense canopy, resulting in an effective decrease in roughness for the dense canopy. As described in Section 2.3, the leaf-level fluxes are affected by the wind speeds inside the canopy through control of conductance across the laminar boundary layer on the leaf surfaces. Greater $\langle U \rangle$ increases the efficiency of removing (or replenishing in the case of CO_2) mass at the leaf surface, thus increasing concentration differences between the internal and external portions of stomatal cavities.

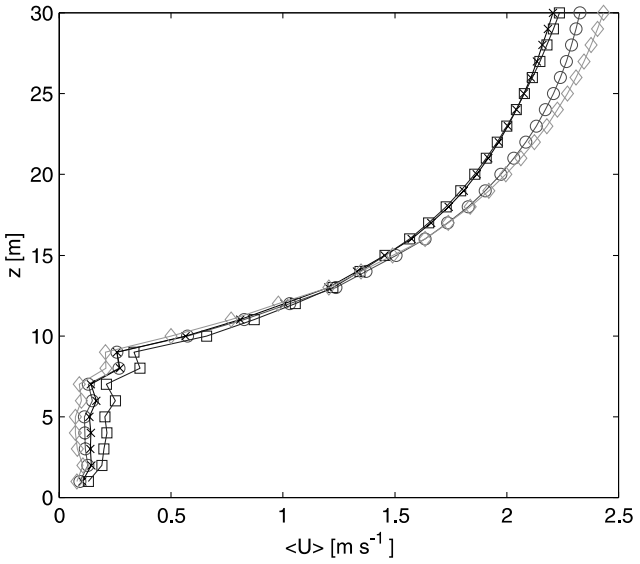

Fig. 2. Mean (horizontal- and time-averaged) profiles of longitudinal wind speed plotted against height in the lower 30 m of the simulation domain. The canopy density shape is distributed vertically according to Fig. 1. The symbols map to the cases as: '×' = heterogeneous, $\langle \mathrm{LAI} \rangle = 5.5$; '□' = homogeneous, LAI = 4; '◯' = homogeneous, LAI = 5.5; '◇' = homogeneous, LAI = 7.

4.2. Scalar exchange in the canopy

In Fig. 3 we present CO_2 exchange and transport results for the region inside the canopy (i.e. $z < 15$ m). In this figure and those following we use m_l^2 to denote leaf area and m_g^2 to denote ground area. Soil processes are not explicitly considered in this study, but to account for soil respiration of CO_2 into the atmosphere, a horizontally homogeneous source strength of 2 μmol m_g^{-2} s^{-1} was assigned at $z = 0$. In the top-left panel of Fig. 3 the mean CO_2 concentration in the main portion of the canopy is seen to decrease with increasing LAI. There is an opposite response near the soil surface, which we attribute to the combined affects of reduced uptake in

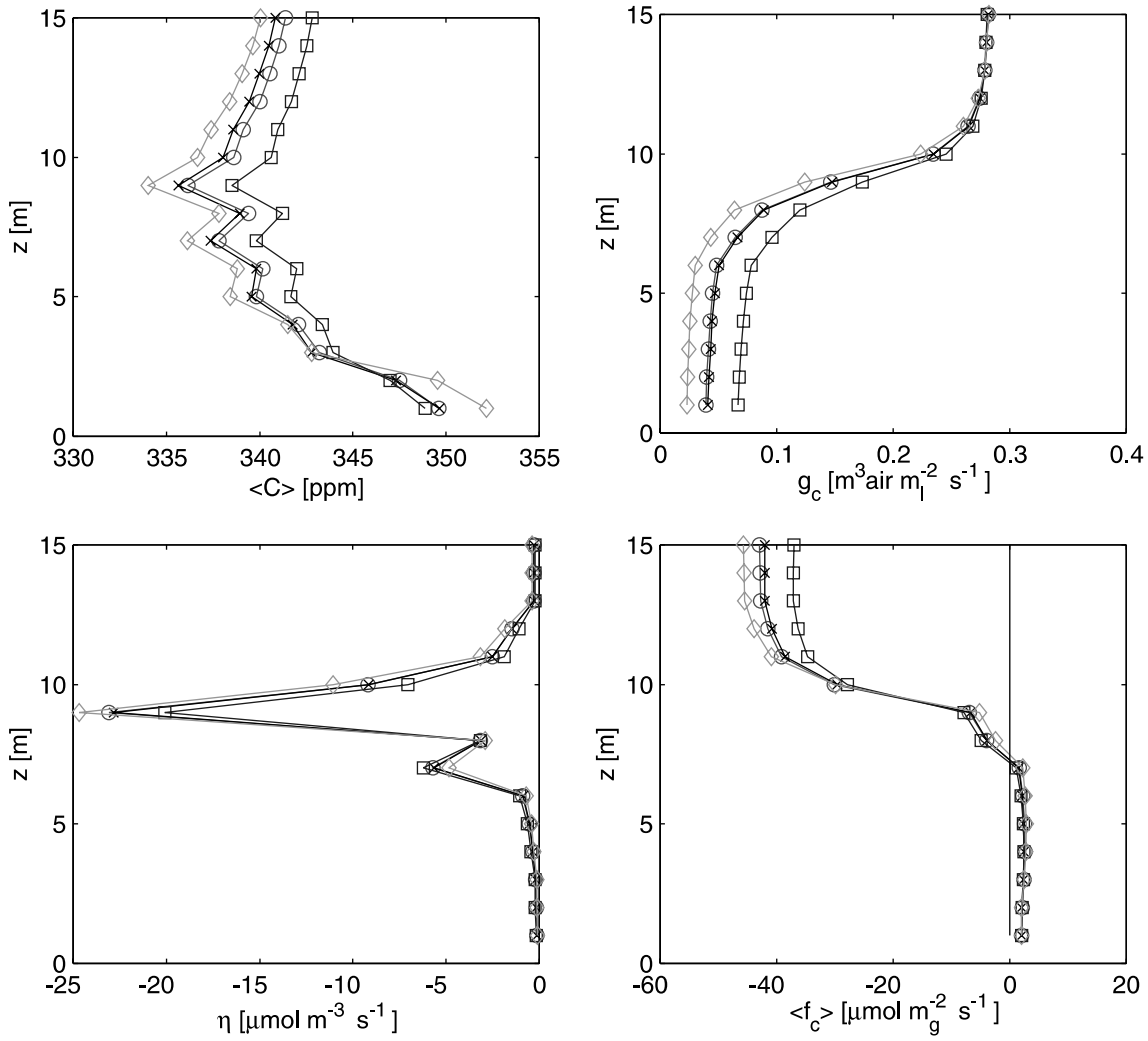

Fig. 3. Mean (horizontal- and time-averaged) profiles related to CO_2 exchange and transport. All symbols are as in Fig. 2. The top-left panel shows the profile of CO_2 concentration in the air. The bottom-left panel is the sink strength (vegetation uptake of CO_2) through the canopy. The top-right panel is the stomatal conductance calculated through the canopy. The bottom-right panel is the mean vertical flux of CO_2 carried by the turbulent flow in the canopy space.

the shaded understory and reduced mixing in the higher LAI cases. In the low LAI case the efficient mixing results in less accumulation of respired CO_2 near the soil surface. In the lower-left panel the mean sink strength of CO_2 (uptake from the air) is shown, as computed by (8)–(14), thus including the instantaneous considerations of PAR, vegetation conditions, CO_2 concentrations in the surrounding air, VPD, and wind speed. The resulting sink strength has features of the vegetation shape profile from Fig. 1, however it is skewed toward stronger sinks in the upper canopy. This is evidenced by the secondary peak in vegetation density realizing only 1/5th of the peak CO_2 uptake while it contains 1/2 the peak vegetation density, as a result of reduced PAR availability in the lower regions of the canopy. The leaf conductance to CO_2 is a byproduct of these calculations and is reported in the top-right panel of Fig. 3. Note that the units are referenced to unit leaf area, such that this profile must be scaled by local foliage density to relate these values to sink strengths. Section 2.3 demonstrates that the conductance is tied to the assimilation rate, and from this point we note for g_c in Fig. 3 that there is a sharp transition from Rubisco controls (i.e. A_{ru} in (8)) in the upper-canopy to PAR control (A_{par}) in the mid- and lower-canopy. This conductance is re-scaled by the ratio of molecular weights (H_2O to CO_2) and used in the transpiration calculations. Hence, the differences in Rubisco and PAR controlled assimilation directly translate into fundamental differences in leaf-level transpiration response to vapor pressure gradients across leaf surfaces. The vertical flux of CO_2 in the flow field (inside the canopy) is shown in the bottom-right panel to be relatively constant with z above the uptake region with a sharp transition to $+2$ μmol m^{-2} s^{-1} below the

dominant uptake region. From 1D mass conservation principles the mean flux at z is equal to the integration of all the mean sources and sinks below z. It is clear from joint inspection of $\langle C \rangle$ and $\langle f_c \rangle$ that the fluxes are not readily described by local gradient diffusion theory. This is examined later, after presentation of results for the remaining scalars.

Mean specific humidity profiles, latent heat source profiles ($\mathrm{LE_c} = \rho_a L_v e$), and the vertical flux fields of latent heat inside the canopy for the four cases are shown in Fig. 4. Clearly, the conductance inferred from the CO_2 processes dominates the source profiles of water vapor to the boundary layer. The vertical latent heat fluxes at the canopy top (i.e. reflecting total canopy contribution) are shown to increase with increasing LAI, while the horizontal heterogeneity in LAI has a negligible impact on the spatial mean latent heat flux (Case 1 compared to Case 3, with like $\langle \mathrm{LAI} \rangle$). Again, the fluxes inside the canopy appear unrelated to local gradients in the mean concentration field, especially below 9 m where the gradient is significant and positive and the fluxes are vanishingly small.

Mean profiles related to sensible heat exchange and transport are shown in Fig. 5. In addition to the types of variables shown for water vapor, here we add mean leaf temperature profiles (top-left) and mean differences between leaf and air temperatures (bottom). The cases with denser canopies have higher leaf temperatures in the upper part of the canopy and lower leaf temperatures in the lower parts of the canopy relative to the sparser canopies. This is due to a more evenly distributed radiation through the canopy under low LAI conditions and the impact of radiation on vegetation temperature through the energy balance of (16). This same crossover of the temperature profiles (for the different cases) in the mid-canopy region is noted for the air temperature. By taking the difference of the leaf and air temperature profiles (bottom panel) we see that the

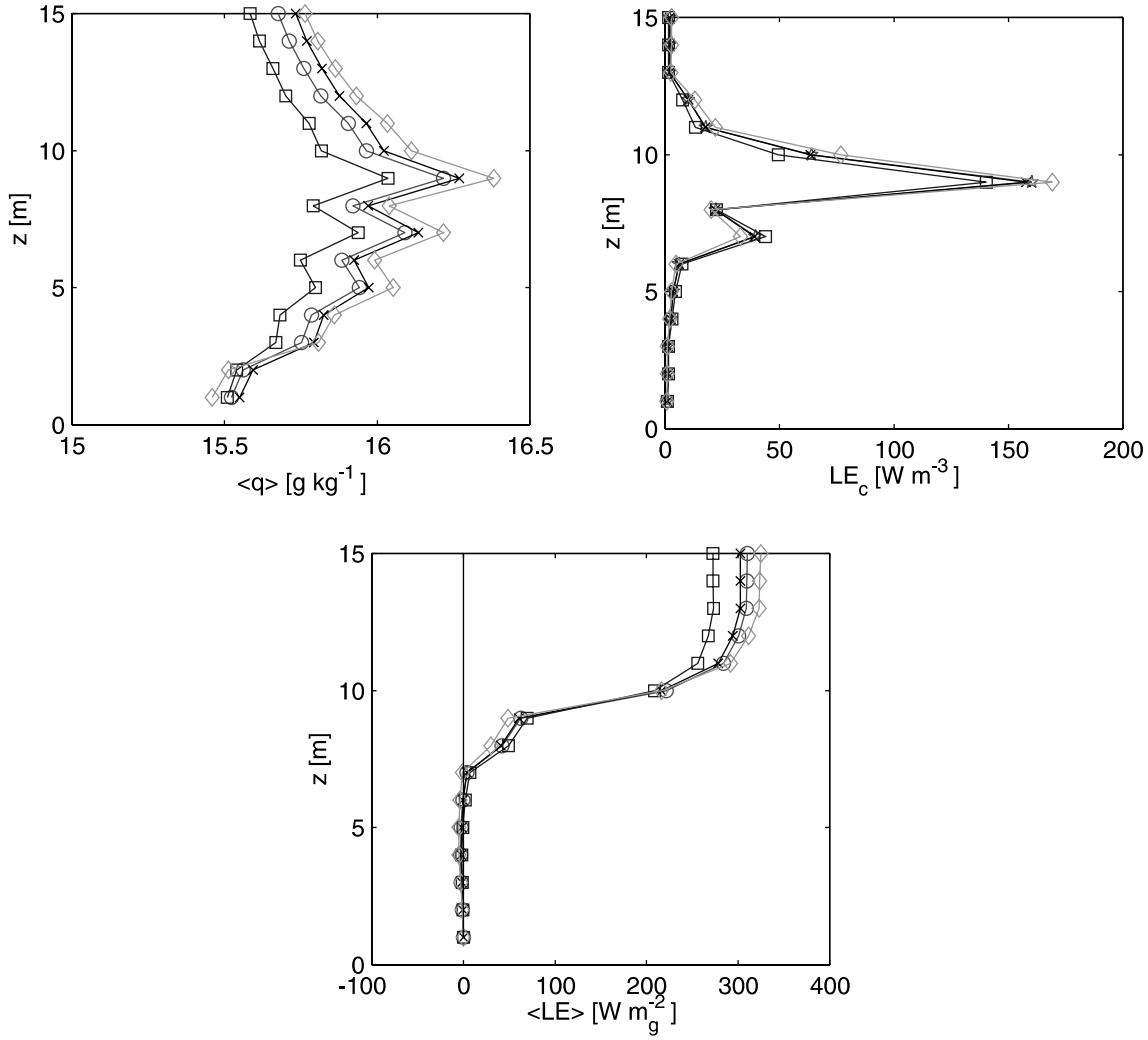

Fig. 4. Mean (horizontal- and time-averaged) profiles related to water vapor exchange and transport. All symbols are as in Fig. 2. The top-left panel shows the profile of water vapor concentration (q) in the air; The top-right panel is the source strength (vegetation's transpiration release) through the canopy. The bottom panel is the mean vertical flux of water vapor carried by the turbulent flow in the canopy space.

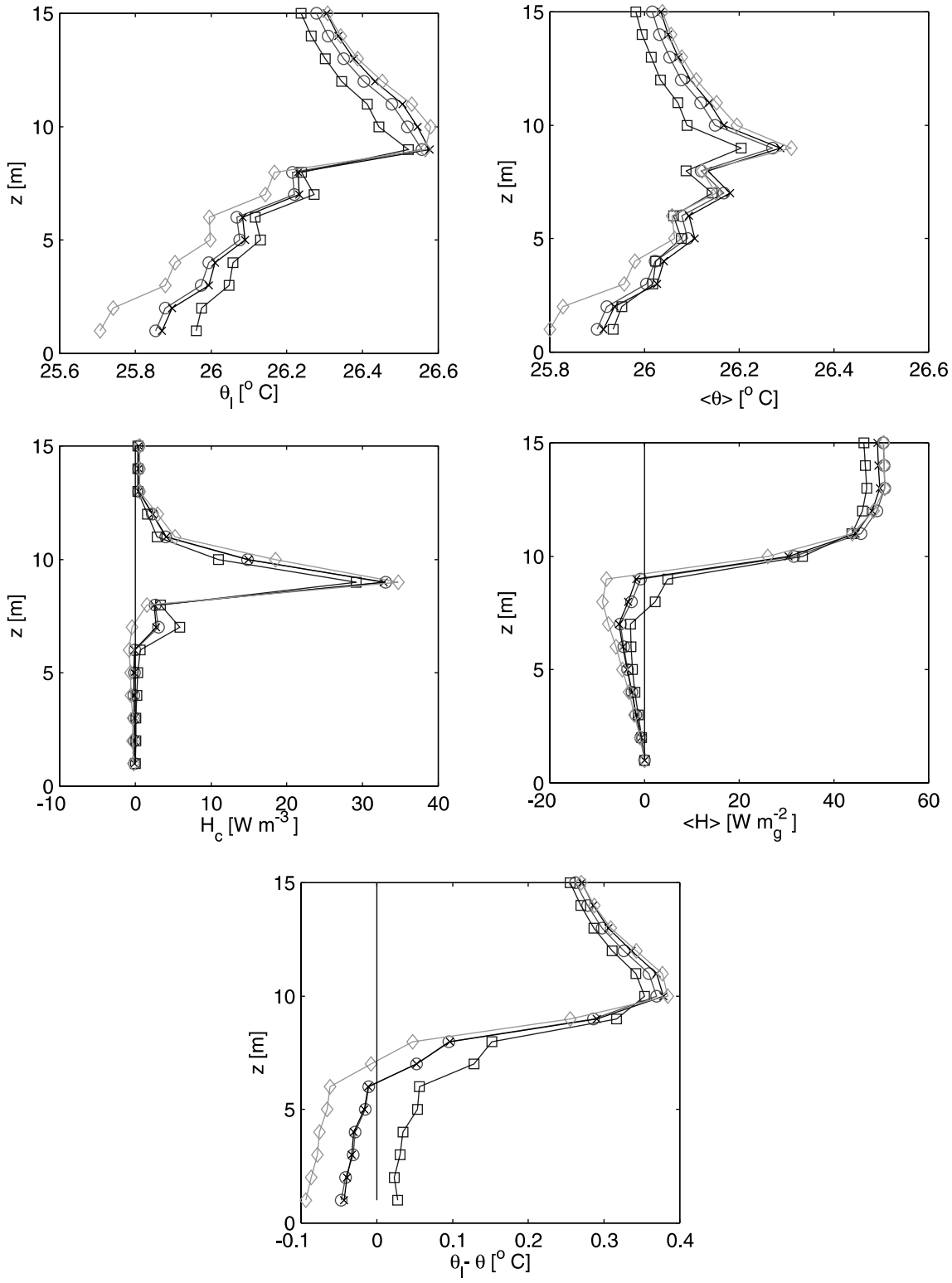

Fig. 5. Mean (horizontal- and time-averaged) profiles related to sensible heat exchange and transport. All symbols are as in Fig. 2. The top-left panel shows the profile of vegetation (leaf) temperature through the canopy depth. The top-right panel shows the profile of air temperature through the canopy depth. The middle-left panel is the source strength of heat to the air through the canopy. The middle-right panel is the mean vertical flux of sensible heat carried by the turbulent flow in the canopy space. The bottom panel is the mean difference between leaf and air temperature through the canopy depth.

denser LAI cases have higher leaf to air temperature differences at the point of peak foliage density, however the denser cases have leaf temperatures in the lower canopy which are lower than local air temperatures. This is in contrast to the LAI = 4 case, which has leaf temperature greater than air temperature at all depths in the canopy. An interesting feedback from these results onto CO_2 and water vapor transport is found in the creation of a stable layer of air in the understory. This positive temperature gradient, $\partial\langle\theta\rangle/\partial z > 0$, acts as a restoring force to vertical air displacements, thus impeding vertical mixing (through the β term in (2)). The downward sensible heat flux indicated in the region of $5\text{ m} < z < 10\text{ m}$ on the bottom-right panel is along the temperature gradient and is balanced by heat exchange from the air to the vegetation (where $\theta_l - \theta < 0$) and the increase in air temperature through time below the main heat source level. The relationship between scalar gradients and turbulent fluxes is considered next.

In Fig. 6 we explore the vertical profiles of the mean turbulent diffusivities for the three scalars as a measure of scalar mixing by the flow field. These profiles are computed as

$$K_s = f_s\left(\frac{\partial\langle S\rangle}{\partial z}\right)^{-1},$$

where K_s is the inferred turbulent diffusivity of scalar S (as proxy for h, v, or c) and f_s is the turbulent vertical flux of scalar S. When modeling (rather than simulating) the turbulence, the turbulent diffusivity is typically estimated as the product of a characteristic turbulent velocity scale and a mixing length scale. In the absence of significant stability effects, the velocity scale is universally considered to be the shear velocity u_*. In the surface layer the mixing length has been shown to be a linear function of height above the zero-plane [49]. Here we see that the combination of small flux magnitudes and significant concentration gradients inside the canopy is representative of vanishingly small turbulent diffusivities inside the canopy. However, just above the canopy we see a non-linear increase in K_s (consistent with roughness sublayer observations) and higher up we recover a mixing length that is linear in z. The failure of gradient diffusion theory inside and often just above plant canopies is well established from field experiments [17]. An encouraging result here is that the three different scalars for all the cases appear to possess similar turbulent diffusivities. To quantify the similarity in source and sink profiles of the three scalars, which is an important determinant in the similarity of transport efficiencies as seen in Fig. 6, we plot the source and sink strengths of the three scalars normalized by their canopy integrated fluxes and the local vegetation density in Fig. 7 (Case 3 only). The shape of the water source and the carbon sink profiles are nearly identical, which we attribute to the strong coupling by stomatal aperture. The heat source profile is noticeably more skewed toward the upper portions of the canopy, however it remains similar enough in shape to the other scalars to result in similar mixing characteristics above the canopy.

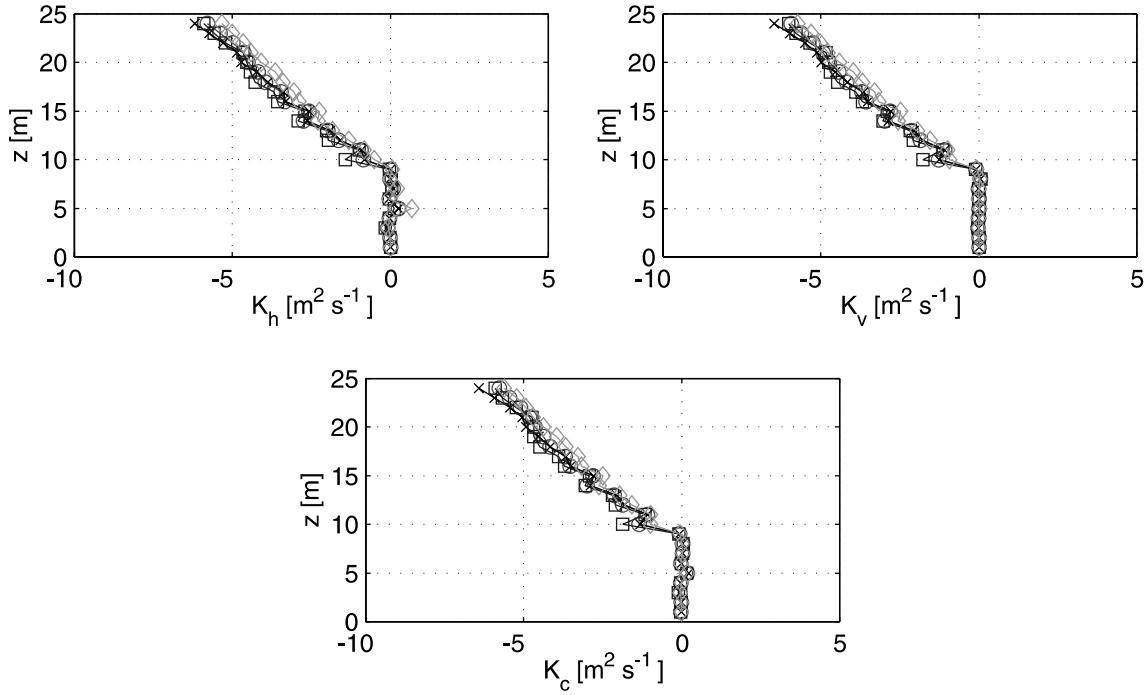

Fig. 6. The inferred mean turbulent diffusivities of heat (K_h), water vapor (K_v) and CO_2(K_c) in and just above the canopy. Symbols are as in Fig. 2.

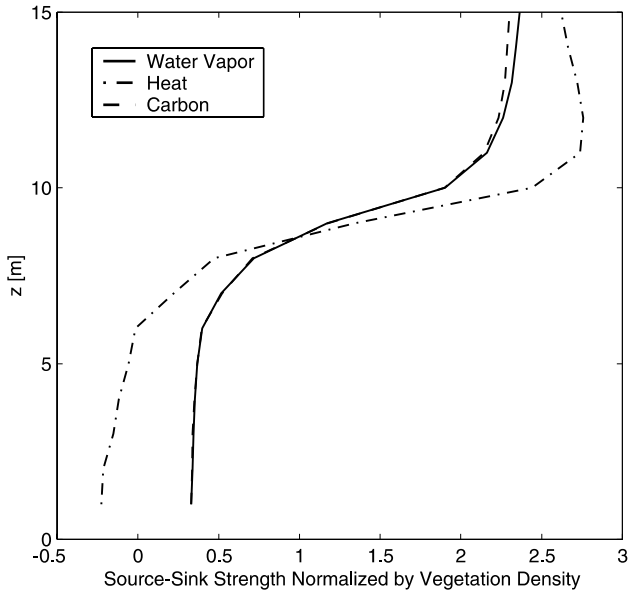

Fig. 7. Relative source/sink strengths versus height in the canopy for heat, water vapor, and CO_2. The source/sink strengths from Figs. 3–5 for the homogeneous-LAI = 5.5 case have been normalized by the total canopy fluxes and by the local vegetation densities to contrast the vertical asymmetry of the canopy exchange processes for the three scalars.

4.3. Global (regional) versus local LAI controls

In Figs. 8 and 9 we explore the relationships between LAI and land surface fluxes and between LAI and canopy environment properties, respectively. For the heterogeneous case (Case 1) we group x, y locations into bins of similar LAI. For each bin we plot the mean dependent variable (e.g. H) and bars denoting ± 1 S.D. of the dependent variable values referenced to the bin. We also plot the global (horizontal) average for the heterogeneous case as an 'x' symbol at LAI = 5.5. The homogeneous cases are plotted as solitary symbols at the appropriate LAI values. The question these figures address is, *'Are the relationships between local LAI and local fluxes and environment variables dependent on the global distribution of LAI throughout the forest*?' As a specific case, is the value of f_c at a location with LAI = 7 in the heterogeneous case (where the forest average LAI is 5.5) the same as that found in a homogeneous case where the local and global mean LAI values are 7 (i.e. Case 4)? This question has important implications for deriving fluxes from distributed data sets using 1D vertical models and then aggregating these model results to regional scales. The findings presented here are limited to short time periods during non-water-limiting conditions and single plant species. Hence, we focus strictly on canopy geometry, leaving the other issues for ongoing and future efforts.

The relationships between the fluxes and LAI values (Fig. 8) are quasi-linear such that the global mean fluxes in the heterogeneous case match the fluxes of the homogeneous case with identical $\langle \mathrm{LAI} \rangle$. The radiation absorption depends functionally on local LAI values. This was justified, as the horizontal length scale over which the LAI varies is greater than the canopy depth. The carbon assimilation and transpiration rates exhibit little scatter about the binned means. The sensible heat flux appears to include minor non-local effects (such as advection), as evidenced by a finite difference between the H values of the heterogeneous and homogeneous cases at LAI = 4 and LAI = 7 (middle-left panel Fig. 8). The carbon assimilation and latent heat fluxes increase similarly to each other with LAI, resulting in a fairly constant canopy water use efficiency (f_c/LE) with LAI. The range of variability in LE and f_c over the heterogeneous LAI distribution is similar to the observed variability in these fluxes from a spatial variability measurement campaign at the Duke Forest [32]. The relatively constant H with LAI interacts with the LE to give a decreasing trend of the Bowen ratio (H/LE) with increasing LAI. The difference in absorbed net radiation across the range of LAI from 4 to 7 results in reduced radiation to the soil in the denser canopy cases. We assume in the present approach, for simplicity, that the soil is a perfect sink for incident energy. While this is clearly not correct, it may not be too detrimental since this soil increment is one order of magnitude smaller than the radiation absorbed by the canopy volume.

The leaf and vegetation properties inside the canopy (Fig. 9) possess more pronounced scatter within each LAI bin, as the state variables are influenced by both local and upwind fluxes through the air flow (advection). These non-local (or regional) controls also lead to greater departure between homogeneous and heterogeneous cases at the same LAI. For example, in the U field a global LAI of 4 (Case 2) yields higher wind speeds than in the regions of the heterogeneous case where LAI = 4 (but with global $\langle \mathrm{LAI} \rangle = 5.5$). The increased wind speeds serve to increase the leaf boundary layer conductance (recall that $g_b \propto \sqrt{\langle U \rangle}$, and hence $\partial g_b / \partial \langle U \rangle \sim \frac{1}{2\sqrt{\langle U \rangle}}$; so with $\langle U \rangle < 1\rangle$, the sensitivity of g_b to $\langle U \rangle$ is significant). This is offset by greater VPDs (top left panel) acting to decrease the canopy conductance (G_c) in the lower-left panel relative to the heterogeneous case. (The canopy conductance is the product of stomatal conductance and leaf area density integrated over the canopy depth.)

These types of offsetting feedbacks serve to translate complicated processes with respect to the state variables into well-constrained behavior of the fluxes. Another excellent example of offsetting effects is found in the vegetation and air temperatures. In Fig. 9 the low LAI conditions of Case 2 result in suppressed air temperatures inside the (well ventilated) canopy compared to low LAI regions of Case 1. A similar result is noted for the

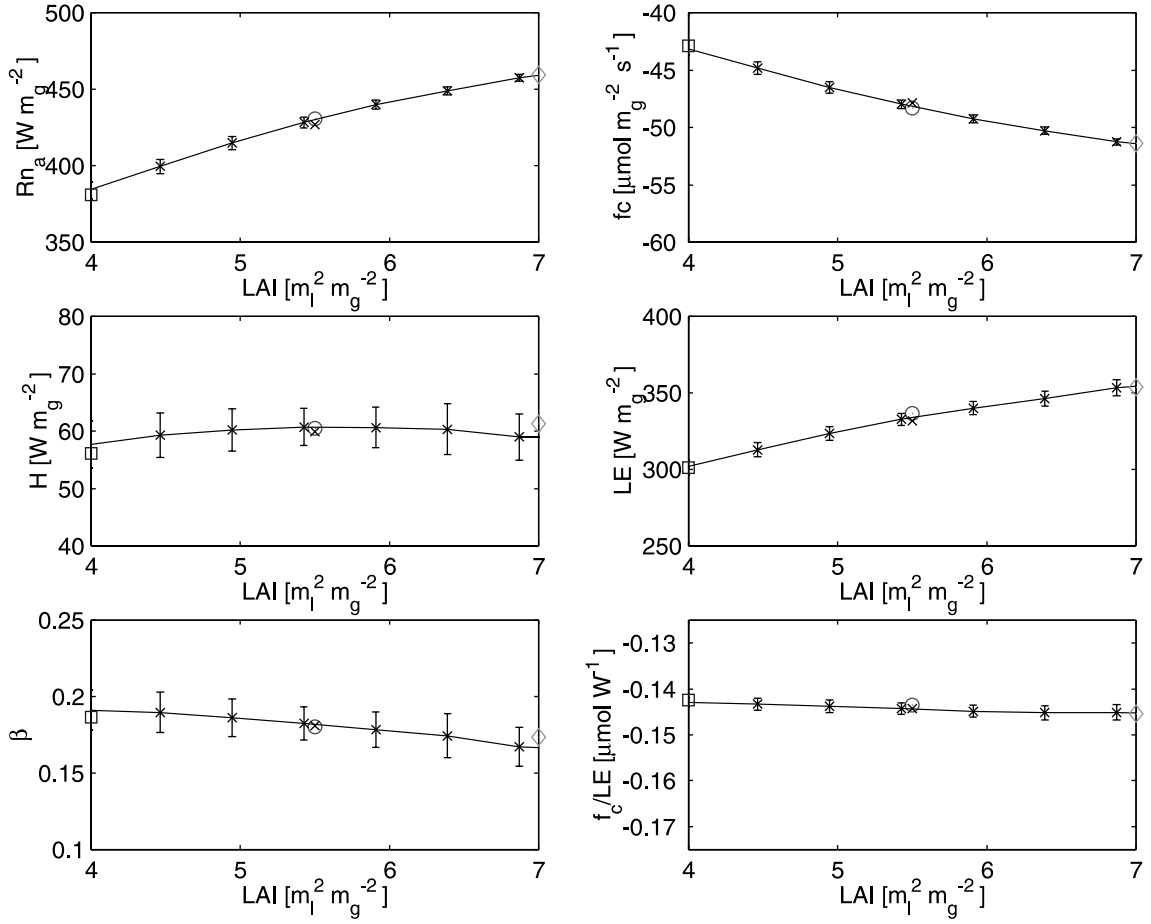

Fig. 8. Binned scatter plots of depth-integrated fluxes in the canopy versus local LAI values. The symbols are as in Fig. 2 and the heterogeneous case includes vertical bars denoting ±1 S.D. of the values in the LAI bin. Each bin includes all x, y locations with LAI values in a range of 0.5 m_l^2 m_g^{-2}. R_{n_a} is the amount of net radiation absorbed by the vegetation; f_c is the net carbon exchange; H is the sensible heat flux; LE is the latent heat flux; β $(= H/\mathrm{LE})$ is the Bowen ratio; and f_c/LE is a measure of the canopies water use efficiency.

leaf temperatures. Hence there are global LAI controls on leaf and canopy air temperature. However, when we focus on the difference between leaf and air temperatures, which drives the heat exchange process, we observe a collapse to local controls (i.e. local LAI values dictate local temperature differences) as evidenced by agreement between homogeneous and heterogeneous simulation results. When $\theta_l - \theta$ is scaled by vegetation density, the resulting heat flux is relatively constant over a wide range of LAI (c.f. middle-left panel of Fig. 8). Therefore, complicated responses of individual primitive variables are offsetting each other to yield simple and robust constraints on fluxes over heterogeneous plant canopies.

At first glance these offsetting feedbacks may appear to be a coincidence or a special case related to the canopy conditions. However, the underlying vegetation strategy suggests otherwise. Recall that the stomatal conductance has been shown to respond to the dual influences of the rates of carbon assimilation [50–52] and water loss [41]. Hence, environmental effects that would serve, for example, to increase transpiration (e.g. increased VPD because of changes to q, θ_l, or θ) will prompt an offsetting response of the stomatal aperture. That is to say, the individual variables do not affect stomatal aperture *independently* but rather *jointly* and weighted in accordance with their influences on rates of water release and/or carbon gain. It is only with the simultaneous treatment of water and carbon cycling that these offsetting effects are so well behaved. As for the sensible heat exchange, we note that leaf temperature responds quickly to maintain a local balance of R_n, H, and LE, and since H is regulated by the difference between leaf and air temperature, it is this difference that must scale well locally. Therefore, the vegetation's water–carbon strategy serves to simplify the flux response. We note that we have addressed a limited spatial region and that magnitudes of departures of state variables from strict local LAI scaling would possibly be greater over larger regions with perhaps greater canopy variability. However, given the discussion of vegetation function strategy we expect that the cancellations would be equally robust as observed here.

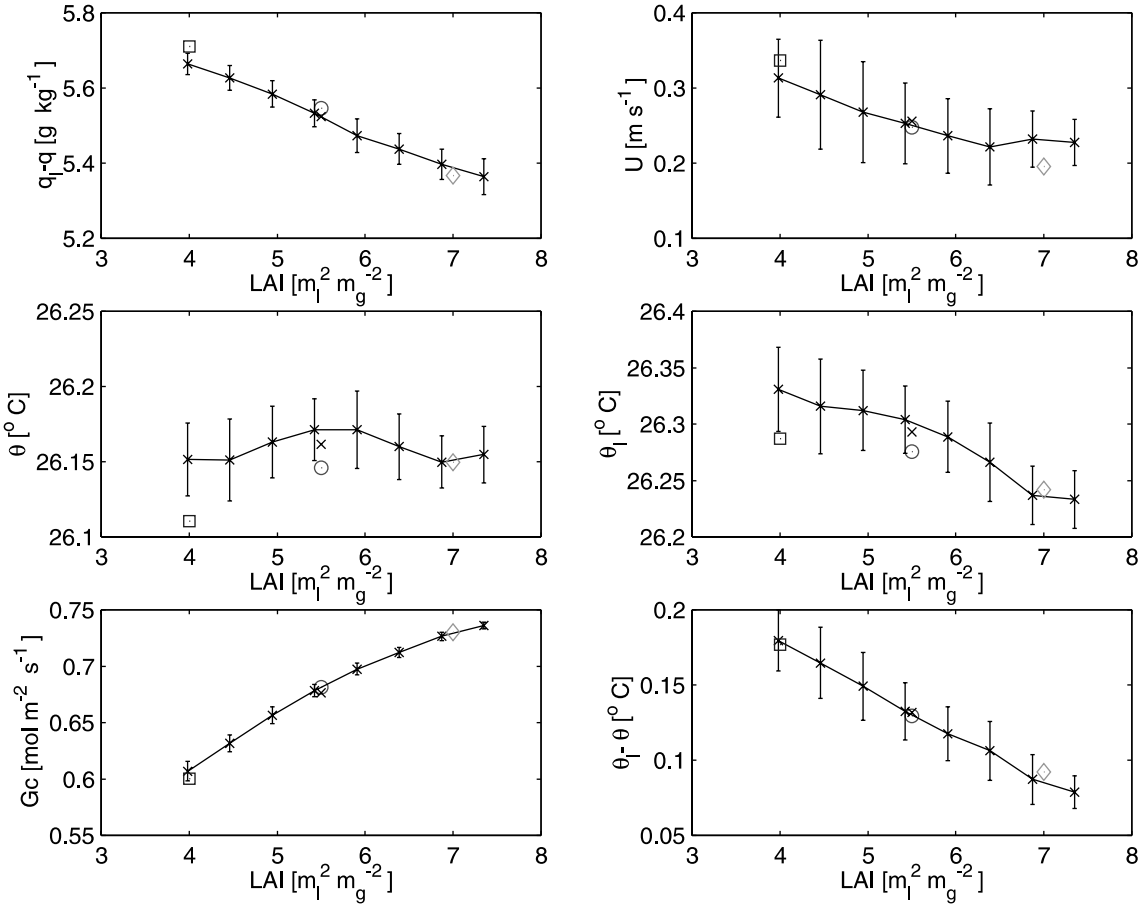

Fig. 9. Binned scatter plots of air and canopy properties averaged over the range of 5 m $< z <$ 10 m and plotted versus LAI values. The symbols are as Fig. 2 and the plot characteristics are as in Fig. 8. $q_l - q$ is the specific humidity difference between leaf and air, U is the wind speed, θ is the air temperature, θ_l is the vegetation temperature, and G_c is the vertically integrated canopy conductance. G_c and LAI are integrated over the full canopy depth all other variables are averaged over the mid-canopy region (5 m $< z <$ 10 m).

5. Conclusions

This study demonstrates that complex interactions between canopy geometry, turbulent transport, and biophysical mechanisms manifest themselves with significant variability in land surface fluxes and moderate variability in concentration fields over a forest of heterogeneous foliage density (LAI ranged from 4 to 7). The vegetation's strategy to maximize carbon uptake while minimizing water loss under prevailing environmental conditions was simulated to deduce 3D, transient fields of stomatal conductance. The conductance controlled the release of water through transpiration, which in turn affected the leaf temperature and sensible heat exchange through a distributed leaf energy balance. The distribution of sensible heat fluxes and the canopy wind field interacted to create density stratification that impeded mixing below the canopy crown (stably stratified) and enhanced mixing above the crown (unstably stratified), with impacts back to the water vapor and CO_2 concentrations inside and above the canopy.

By comparing a simulation of a horizontally heterogeneous canopy and simulations of three homogeneous canopies (with different LAI values) we were able to discern the relative importance of local LAI and global (regional) LAI controls on local concentrations and fluxes. For this single species example under non-water-limiting conditions, it was demonstrated that concentrations (e.g. q, θ) and velocities (i.e. state variables) exhibited noticeable non-local controls while the land surface fluxes did not. This is attributed to negative feedback pathways (offsetting effects) between stomatal and boundary layer conductance, as suggested in the theoretical work of Jarvis and McNaughton [27], with reduced (increased) wind speeds acting to lower (increase) the boundary layer conductance which increases (decreases) water vapor concentrations at leaf surfaces thus decreasing (increasing) VPD and increasing (decreasing) the stomatal conductance. In fact, since the stomatal response is to the *rate* of carbon assimilation [50–52] and the *rate* of water loss [41] it is predictable that an external perturbation that increases transpirative loss should be equally offset by an equivalent stomatal

restriction to maintain the desired water/carbon balance. Hence, the various state variables affecting the conductance do not act independently, but rather in a joint matter defined by their relative effects on transpiration (and carbon assimilation) – apparently leading to a robust water use efficiency that does not vary appreciably with local environmental perturbations. We demonstrate other offsetting effects here as well, such as the cancellation of non-local controls on leaf temperature and air temperature to result in a simple local scaling of the 'difference between leaf and air temperature', as used in the estimation of sensible heat exchange. This should also be a general truth given that the leaf temperature responds rapidly (low foliage heat capacity) to maintain a balance between local net radiation and latent and sensible heat fluxes. So, given an LAI -defined net radiation and latent heat loss the leaf temperature would have to adjust relative to the air temperature to yield the appropriate leaf-to-air temperature difference to dissipate the residual heat – hence, the simple local scaling of '$\theta_l - \theta$' – a direct consequence of the leaf energy balance.

In the presence of ample soil moisture, uniform solar radiation and species composition, the land surface fluxes scale quasi-linearly with LAI over the LAI encountered here, such that the forest average fluxes are well described by the forest average LAI and are thus insensitive to the horizontal variability of LAI. There are interesting implications for efforts aiming to compute distributed fluxes and scale to the region. We surmise that results from such efforts may have greatest likelihood of success at the two extreme ends of the dimensionality of the models. The simple models that ignore impacts of forest heterogeneity on the state variables may recover the correct solution and detailed process models (such as this LES with dynamic canopy) may capture all the variability and the offsetting effects, yet models that partially treat the complications are likely to fail to capture the full counteraction of the jointly acting variables. An example of a complication (and possible source of error) for a mid-range complexity model would be accurately dealing with satellite derived canopy temperature data $(\theta_l(x,y))$ in the absence of spatially distributed air temperature data $(\theta(x,y))$.

The encouraging finding for regions represented by ample water supply is that despite all the complications within the forest, the regional scale exchange is regulated more by vegetation response to large scale energy input and vegetation density in the context of an optimum coupling of the carbon, water, and energy cycles.

Acknowledgements

This research was funded by the National Institute for Global Environmental Change (NIGEC) through the US Department of Energy (Cooperative Agreement No. DE-FC03-90ER61010) by a grant to the University of Virginia and by a grant from the National Science Foundation's WEAVE and Hydrologic Science programs (EAR-9902957.)

References

[1] Albertson JD. Large-eddy simulation of land–atmosphere interaction. PhD Thesis, University of California, Davis, 1996, 185 pp.
[2] Albertson JD, Parlange MB. Surface length scales and shear stress: implications for land–atmosphere interaction over complex terrain. Water Resour Res 1999a;35:2121–32.
[3] Albertson JD, Parlange MB. Natural integration of scalar fluxes from complex terrain. Adv Water Resour 1999b;23:239–52.
[4] Albertson JD, Kustas WP, Scanlon TM. Large-eddy simulation over heterogeneous terrain with remotely sensed land surface conditions. Water Resour Res 2001;37:1939–53.
[5] Andren A, Brown AR, Graf J, Mason PJ, Moeng C-H, Nieuwstadt FTM, Schumann U. Large-eddy simulation of a neutrally stratified boundary layer: a comparison of four computer codes. QJR Meteorol Soc 1994;120:1457–84.
[6] Aphalo PJ, Jarvis PG. Do stomata respond to relative humidity. Plant Cell Environ 1991;14:127–32.
[7] Avissar R. Scaling of land–atmosphere interactions: an atmospheric modelling perspective. Hydrol Process 1995;9:679–95.
[8] Avissar R, Schmidt T. An evaluation of the scale at which ground-surface heat flux patchiness affects the convective boundary layer using large-eddy simulation. J Atmos Sci 1998;55:2666–89.
[9] Ball JT, Woodrow IE, Berry JA. A model predicting stomatal conductance and its contribution to the control of photosynthesis under different environmental conditions. In: Biggens J, editor. Progress in photosynthesis research, vol. IV. 1987. p. 221–4.
[10] Brusaert W. In: Evaporation into the atmosphere: theory, history, and applications. Dordrecht: Kluwer Academic Publishers; 1982, 299 pp.
[11] Campbell GS, Norman JM. An introduction to environmental biophysics. Berlin: Springer; 1998. 286 pp.
[12] Cescatti A. Modeling the radiative transfer in discontinuous canopies of asymmetric crowns, 1: Model structure and algorithms. Ecol Modeling 1997;101:263–74.
[13] Collatz CJ, Ball JT, Grivet C, Berry JA. Physiological and environmental regulation of stomatal conductance, photosynthesis, and transpiration: a model that includes a laminar boundary layer. Agric For Meteorol 1991;54:107–36.
[14] Cowan IR, Farquhar GD. Stomatal function in relation to leaf metabolism and environment. In: Jennings DH, editor. Integration of Activity in the Higher Plant, SEB Symposium XXXI. Cambridge, UK: Cambridge University Press; 1977. p. 471–505.
[15] Deardorff JW. Preliminary results from numerical integrations of the unstable planetary boundary layer. J Atmos Sci 1970a;27:1209–11.
[16] Deardorff JW. Convective velocity and temperature scales for the unstable planetary boundary layer and Rayleigh convection. J Atmos Sci 1970b;27:1213–33.
[17] Denmead OT, Bradley EF. Flux-gradient relationships in a forest canopy. In: Hutchinson BA, Hicks BB, editors. The forest–atmosphere interaction. Norwell, MA: D. Reidel; 1985. p. 421–42.
[18] De Pury DGG, Farquhar GD. Simple scaling of photosynthesis from leaves to canopies without the errors of big-leaf models. Plant Cell Environ 1997;20:537–57.
[19] Dwyer MJ, Patton EG, Shaw RH. Turbulent kinetic energy budgets from a large-eddy simulation of airflow above and within a forest canopy. Boundary-Layer Meteorol 1997;84(1):23–43.

[20] Ellsworth D, Oren R, Huang C, Phillips N, Hendrey GR. Leaf and canopy responses to elevated CO_2 in a pine forest under free air CO_2 enrichment. Oecologia 1995;104:139–46.
[21] Ellsworth DS. CO_2 enrichment in a maturing pine forest: are CO_2 exchange and water status in the canopy affected?. Plant Cell Environ 1999;22:461–72.
[22] Farquhar GD, von Caemmerer S, Berry JA. A biochemical model of photosynthetic CO_2 assimilation in leaves of C_3 species. Planta 1980;149:78–90.
[23] Farquhar GD, von Caemmerer S. Modeling of photosynthetic response to environmental conditions. In: Lange OL, Nobel PS, Osmond CB, editors. Encyclopedia of plant physiology, New Series, vol. 12B. Berlin: Springer; 1982. p. 549–87.
[24] Hechtel LM, Moeng C-H, Stull RB. The effects of nonhomogeneous surface fluxes on the convective boundary layer: a case study using large-eddy simulation. J Atmos Sci 1990;47:1722–41.
[25] Hipps LE, Swiatek E, Kustas WP. Interactions between regional surface fluxes and the ABL over a heterogeneous watershed. Water Resour Res 1994;30:1387–92.
[26] Jarvis PG. The interpretation of the variations in leaf water potential and stomatal conductance found in canopies in the field. Philos Trans R Soc London, Ser B – Biol Sci 1976;273:593–610.
[27] Jarvis PG, McNaughton KG. Stomatal control of transpiration: scaling up from leaf to region. Adv Ecol Res 1986;15:1–49.
[28] Jordan D.B, Ogren WL. The CO_2/O_2 specificity of ribulose 1,5-bisphosphate carboxylase/oxygenase: dependence on ribulose bisphosphate concentration, pH and temperature. Planta 1984;161:308–13.
[29] Katul GG, Albertson JD. An investigation of higher order closure models for a forested canopy. Boundary-Layer Meteorol 1998;89:47–74.
[30] Katul GG, Albertson JD. Modeling CO_2 sources, sinks, and fluxes within a forested canopy. J Geophys Res – Atmos 1999;104(D6):6081–92.
[31] Katul GG, Ellsworth D, Lai CT. Modeling assimilation and intercellular CO_2 from measured conductance: a synthesis of approaches. Plant Cell Environ 2000;23(12):1313–28.
[32] Katul GG, Hsieh CI, Bowling D, Clark K, Shurpali N, Turnipseed A, Albertson JD, Tu K, Hollinger D, Evans B, Offerle B, Anderson D, Ellsworth D, Vogel C, Oren R. Spatial variability of turbulent fluxes in the roughness sublayer of an even-aged pine forest. Boundary-Layer Meteorol 1999;93:1–28.
[33] Krettenauer K, Schumann U. Numerical simulation of turbulent convection over wavy terrain. J Fluid Mech 1992;237:261–99.
[34] Lai C-T, Katul G, Ellsworth D, Orenx R. Modeling vegetation–atmosphere CO_2 exchange by a coupled Eulerian–Langrangian approach. Boundary-Layer Meteorol 1984;95:91–122.
[35] Leuning R. A critical appraisal of a combined stomatal-photosynthesis model for C_3 plants. Plant Cell Environ 1995;18:339–55.
[36] McNaughton KG, Jarvis PG. Effects of spatial scale on stomatal control of transpiration. Agric For Meteorol 1991;54:279–301.
[37] Medlyn BE, Badeck F-W, de Pury DGG, Barton CVM, Broadmeadow M, Ceulemans R, de Angelis P, Forstreuter M, Jach ME, Kellomaki S, Laitat E, Marek M, Phillippot S, Rey A, Strassmeyer J, Laitinen K, Loizon R, Portier B, Roberntz P, Wang K, Jarvis PG. Effects of elevated CO_2 on photosynthesis in European forest species: a meta-analysis of model parameters. Plant Cell Environ 1999;23:1475–96.
[38] Moeng C-H. A large-eddy-simulation model for the study of planetary boundary-layer turbulence. J Atmos Sci 1984;41:2052–62.
[39] Moin P, Reynolds WC, Feringer JH. Large-eddy simulation of incompressible turbulent channel flow. Rep. TF-12, Department of Mechanical Engineering, Stanford University, Stanford, CA, 1978.
[40] Mott KA. Do stomata respond to CO_2 concentrations other than intercellular?. Plant Physiol 1988;86:200–3.
[41] Mott KA, Parkhurst DF. Stomatal responses to humidity in air and helox. Plant Cell Environ 1991;14:509–15.
[42] Oren R, Phillips N, Katul GG, Ewers BE, Pataki D. Scaling xylem sapflux and soil water balance and calculating variance: a method for partitioning water flux in forests. Ann Sci For 1998;55:191–216.
[43] Raupach MR. Canopy transport processes. In: Steffen WL, Denmead OT, editors. Flow and transport in the natural environment. Berlin: Springer; 1988. p. 95–127.
[44] Raupach MR, Thom AS. Turbulence in and above plant canopies. Ann Rev Fluid 1981;13:97–129.
[45] Shaw RH, Schumann U. Large-eddy simulations of turbulent flow above and within a forest. Boundary-Layer Meteorol 1992;61:47–64.
[46] Shen S, Leclerc MY. How large must surface inhomogeneities be before they influence the convective boundary layer structure: a case study. QJR Meteorol Soc 1995;121:1209–28.
[47] Shen S, Leclerc MY. Modeling the turbulence structure in the canopy sublayer. Agric For Meteorol 1997;87:3–25.
[48] Su HB, Shaw RH, Paw UKT. Two-point correlation analysis of neutrally stratified flow within and above a forest from large-eddy simulation. Boundary-Layer Meteorol 2000;94(3):423–60.
[49] Tennekes H, Lumley JL. A first course in turbulence. Cambridge: MIT Press; 1972. 300 pp.
[50] Wong S-C, Cowan IT, Farquhar GD. Leaf conductance in relation to rate of CO_2 assimilation: I. influence of nitrogen nutrition, phosphorus nutrition, photon flux density, and ambient partial pressure of CO_2 during ontogeny. Plant Physiol 1985a;78:821–5.
[51] Wong S-C, Cowan I, Farquhar GD. Leaf conductance in relation to rate of CO_2 assimilation: II. Effects of short-term exposures to different photon flux densities. Plant Physiol 1985b;78:826–9.
[52] Wong S-C, Cowan I, Farquhar GD. Leaf conductance in relation to rate of CO_2 assimilation: III. Influences of water stress and photoinhibition. Plant Physiol 1985c;78:830–4.
[53] Yang R, Friedl MA, Ni W. Parameterization of shortwave radiation fluxes for nonuniform vegetation canopies in land surface models. J Geophys Res – Atmos 2001;106(D13):14275–86.